Shape Optimization of Three-Dimensional Continuum Structures via Force Approximation Techniques

Srinivas Kodiyalam*
Engineering Design Optimization, Inc., Santa Barbara, California
and
Garret N. Vanderplaats†
University of California, Santa Barbara, California

The existing need to develop methods whereby the shape design efficiency can be improved through the use of high-quality approximation methods is addressed. An efficient approximation method for stress constraints in three-dimensional shape design problems is proposed, based on expanding the nodal forces in Taylor series with respect to shape variations. The significance of this new method is shown through elementary beam theory calculations and via numerical computations using three-dimensional solid finite elements. Numerical examples, including the classical cantilever beam structure and realistic automotive parts like the engine connecting rod, are designed for optimum shape using the proposed method. The numerical results obtained from these methods are compared with other published results to assess the efficiency and the convergence rate of the proposed method. It is concluded that, by taking advantage of this high-quality approximation, the total number of finite-element analyses required for structural shape optimization can be reduced significantly, resulting in the same level of efficiency achieved previously in sizing problems.

Introduction

CONSIDERABLE effort has been directed toward finding the optimum shape of continuum structures by varying the finite-element (joint) coordinates. As a result of inherent nonlinearities, shape optimization of complex, large-scale three-dimensional strucures is a difficult task as compared to gage sizing problems.

Three-dimensional solid modeling involves a large number of degrees of freedom and complex elements, and a single finite-element analysis of the structure requires a significant amount of computer time. Hence, approximate evaluation of the structural responses for perturbed designs has become a critical element of the optimization algorithm in order to avoid many complete finite-element anlayses.

The characteristics of approximations, such as applicable range in the design variable space, conservativeness, separability of mathematical representations, and convexity, have been investigated to improve the overall numerical efficiency.[1] In Ref. 1, the primal problem has been replaced by the dual mathematical programming statement and the resulting problem solved in terms of the dual variables.

In Ref. 2, a new method was proposed to obtain high-quality stress approximations by expanding internal forces in Taylor series with respect to sizing variables. The improved results obtained in Ref. 2 were attributed to the fact that stress approximations thus obtained are, in fact, higher-order approximations compared to direct Taylor series approximations of stresses. In this study, the concept proposed in Ref. 2 has been extended to create improved approximations of stresses in three-dimensional solid elements with respect to shape variations, and these approximations are used to optimize general three-dimensional structural shapes, resulting in significantly improved convergence characteristics. However, unlike skeletal structures, nodal forces are not directly obtained in plane and solid continuum elements. Hence, at the approximate problem level, an elemental approach has been used. The method presented here is based on the work of Ref. 3.

Yang and Botkin[4] have used a material derivative approach for shape sensitivities to solve shape optimization problems. Some of their examples are used in this study to compare the efficiency and convergence rate of the proposed method.

Mathematical Problem Statement

The mathematical programming problem is stated as follows:
Minimize:

$$F(X) \qquad \text{objective function}$$

Subject to:

$$g_j(X) \le 0, \quad j = 1, m \qquad \text{inequality constraints}$$
$$x_i^l \le x_i \le x_i^u, \quad i = 1, n \qquad \text{side constraints} \tag{1}$$

where X is the vector of design variables.

In the shape optimal design problem considered here, the objective function is the volume of the structure, and constraints are imposed on the von Mises equivalent stresses, normal stresses, or octahedral shear stresses at various locations in the finite elements. Side constraints are also imposed on the design variables, which are the nodal coordinates of key locations of the structure.

Present Method

An analysis of the structure is performed to compute the initial volume and the static responses of the structure. The nodal forces are then obtained from the element stiffness equations:

$$[K^e]\{u^e\} = \{F^e\} \tag{2}$$

Presented as Paper 88-2437 at the AIAA/ASME/ASCE/AHS 29th Structures, Structural Dynamics and Materials Conference, Williamsburg, VA, April 18–20, 1988; received June 1, 1988; revision received Oct. 16, 1988.

*Research Engineer.
†Professor, Department of Mechanical and Environmental Engineering. Associate Fellow AIAA.

where $[K^e]$ is the element stiffness matrix, $\{u^e\}$ the vector of nodal displacements, and $\{F^e\}$ the vector of element nodal forces. In this approximation, the element nodal forces (F^e) are updated for every change in design through a first-order Taylor series expansion. This requires the gradient of the nodal forces with respect to the shape variables. This could be computed as

$$\frac{\partial F^e}{\partial x_i} = K^e \frac{\partial u^e}{\partial x_i} + \frac{\partial K^e}{\partial x_i} u^e, \quad i = 1, \text{ ndv} \tag{3}$$

where ndv is the number of design variables, and the term $\partial u^e/\partial x_i$ is obtained from differentiating the overall structural equilibrium equations:

$$[K]\{u\} = \{P\} \tag{4}$$

$$\frac{\partial u}{\partial x_i} = K^{-1}\left[\frac{\partial P}{\partial x_i} - \frac{\partial K}{\partial x_i} u\right], \quad i = 1, \text{ ndv} \tag{5}$$

The force sensitivity obtained from Eq. (3) is then used to obtain linear approximations to the element nodal forces. For every change in design:

$$F_1^e(\boldsymbol{X}) = F^e(\boldsymbol{X}_0) + \sum_{i=1}^{\text{ndv}} \frac{\partial F^e(\boldsymbol{X}_0)}{\partial x_i} \delta x_i \tag{6}$$

where $\delta x_i = x_i - x_{0i}$ and $\boldsymbol{X}_0$ represents the vector of initial design variables. The element stiffness matrix (K_1^e) and the strain displacement matrix (B_1^e), corresponding to the changes in the finite-element mesh, can be either rebuilt or approximated through a first-order Taylor series expansion.

For every change in design, the element joint displacements $\{u_1^e\}$ are computed from

$$[K_1^e]\{u_1^e\} = \{F_1^e\} \tag{7}$$

The element stiffness matrix K_1^e is singular, and hence this equation cannot be solved directly. In order to remove the singularity, the rigid-body degrees of freedom must be removed. In the case of curved elements, it is difficult to ascertain the number and form of rigid-body modes contained in the stiffness matrix.[5] By transforming the element stiffness matrix to a diagonal matrix through congruent transformations, the number of zero diagonal terms gives the number of rigid-body modes. Jacobi's iterative method,[6] which operates on a real, symmetric matrix to reduce it to a diagonal form, is used here:

$$[K^d] = [T]^T[K_1^e][T] \tag{8}$$

where $[K^d]$ is the diagonalized stiffness matrix and $[T]$ the rotation matrix used in the Jacobi technique to reduce the off-diagonal terms to zero.

An alternate method to remove the singularity in the element stiffness matrices is to choose a set of six translational degrees of freedom as rigid-body modes. It is generally advantageous to choose the first three rigid-body modes as three orthogonal degrees of freedom at a node, while the three remaining may be selected in many different ways. In civil engineering structures, this latter choice is often governed by the degrees of freedom, which are restrained by the rigid foundation to which the structure is attached.[7]

Once the rigid-body modes are detected and removed, Eq. (7) can be solved to obtain $\{u_1^e\}$.

As outlined earlier, within the approximate problem, the stiffness equations are solved at the element level, thereby eliminating the need to form a master stiffness matrix. Considerable computational time is saved by eliminating the need to solve a large system of equations and restricting to an n number of solutions of 54×54 equations (for 20 node elements with rigid-body degrees of freedom eliminated). Here n represents the total number of elements in the finite-element model, each node having 3 translational degrees of freedom.

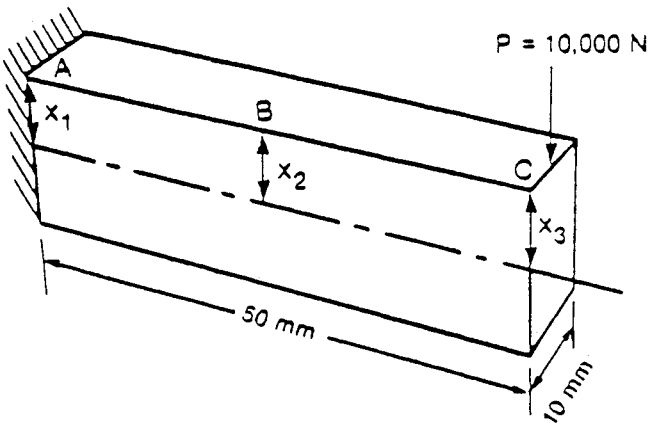

Fig. 1. Three-dimensional cantilever beam.

The displacements $\{u_1^e\}$ obtained from Eq. (7) are then used to compute the normal and shear stresses at various locations in the element:

$$\{\sigma^e\} = [D^e][B_1^e]\{u_1^e\} \tag{9}$$

where $[D^e]$ is the element material property matrix and $[B_1^e]$ the strain displacement matrix. For the case where von Mises equivalent stresses are used, these are then calculated from

$$\sigma_{\text{V.M.}} = (1/\sqrt{2})[(\sigma_x - \sigma_y)^2 + (\sigma_y - \sigma_z)^2 + (\sigma_z - \sigma_x)^2 + 6\tau_{xy}^2 + 6\tau_{yz}^2 + 6\tau_{zx}^2]^{\frac{1}{2}} \tag{10}$$

If octahedral shear stresses are used, these are obtained from

$$\sigma_{\text{oct}} = (\sqrt{2}/3)\sigma_{\text{V.M.}} \tag{11}$$

Finally, the approximate stress constraints are given by

$$\tilde{g} = (\sigma_{\text{V.M.}}/\sigma_{\text{allowable}}) - 1 \leq 10 \tag{12}$$

Significance of the Proposed Method

The major difference between the proposed method and previous methods for generation of the approximate problem is that here the approximate stresses are obtained through linearization of the nodal forces rather than by direct linearization of the stresses. The stress approximations obtained by expanding the nodal forces in Taylor series with respect to shape variation can be shown, in fact, as higher-order approximations through the following simple example.

Consider a structure made of rectangular beam elements of width b and height h (Fig. 1). From elementary strength of materials, the maximum bending stress is

$$\sigma = \frac{Mc}{I} = \frac{M(h/2)}{bh^3/12} = \frac{6M}{bh^2} \tag{13}$$

Now creating a first-order Taylor series approximation for stress, in terms of the design variables b and h,

$$\tilde{\sigma} = \sigma^0 + \left(\frac{6}{bh^2}\frac{\partial M}{\partial h} - \frac{12M}{bh^3}\right)\delta h + \left(\frac{6}{bh^2}\frac{\partial M}{\partial b} - \frac{6M}{b^2h^2}\right)\delta b \tag{14}$$

Clearly, this is highly nonlinear in n and b, even for statically determinate structures (in which case $\partial M/\partial h = 0$ and $\partial M/\partial b = 0$). Now approximate only the bending moment in terms of h and b:

$$\tilde{M} = M^0 + \frac{\partial M}{\partial h}\delta h + \frac{\partial M}{\partial b}\delta b \tag{15}$$

The stress is now calculated as

$$\tilde{\sigma} = \frac{6[M^0 + (\partial M/\partial h)\delta h + (\partial M/\partial b)\delta b]}{bh^2} \tag{16}$$

where h and b are the current values of the design variables, during the approximate optimization. Now, for statically determinate structures ($\partial M/\partial h = 0$ and $\partial M/\partial b = 0$), Eq. (16) is precise. Thus, Eq. (16) is clearly a higher-order approximation to the stress than Eq. (14).

The key point here is that the stress recovery calculations themselves contain significant nonlinearities, which need not be approximated using the present method. Thus, although it is not possible to construct such a simple example for general continuum structures, the basic concept is the same and must be demonstrated through examples.

Numerical computations were done to see how well the approximate stresses, obtained through the linearization of nodal forces, the direct linearization of the stresses, and the convex linearization approach,[8] compared with the true stresses using three-dimensional finite elements. The procedure is outlined as follows:

1) Compute $\{\sigma^0\}$ through a detailed finite-element analysis, at the initial design $\boldsymbol{X}_0$.

2) Compute the gradient of the nodal forces $(\partial F^e(\boldsymbol{X}_0)/\partial x_i)$ and the gradient of the stresses $(\partial\sigma(\boldsymbol{X}_0)/\partial x_i)$ (here x_{0i} represents the initial design vector; $i = 1$, number of design variables).

3) Compute $\{\sigma_f^0\}$, $\{\sigma_s^0\}$, and $\{\sigma_c^0\}$, the stresses corresponding to the initial design, through the force approximation, the stress approximation, and convex linearization, respectively.

4) Perturb the design variables [1, 5, 10, 20, 25, and 50%]: perform a detailed analysis to obtain the true stresses at each of the preceding values, and compute $\{\sigma_f\}$, $\{\sigma_s\}$, and $\{\sigma_c\}$ for each of the preceding perturbations.

5) Compute the error in $\{\sigma_f\}$ $\{\sigma_s\}$, and $\{\sigma_c\}$ with respect to the "true" stress obtained through a detailed finite-element analysis.

The cantilever beam (Fig. 1), modeled with three design variables, is considered as the test example. The shape of the beam is determined as a quadratic curve fit through these points. In each example, the error indicates an underestimate of the true stress.

Case 1

The design variable x_1, corresponding to the height of the cantilever beam at the wall, is perturbed. The percent error in $\{\sigma_f\}$, $\{\sigma_c\}$ and $\{\sigma_s\}$ with respect to the true stress, at the support location where the structure is maximum stressed, is listed in Table 1; Fig. 2 shows a plot of the results.

Case 2

The design variable x_2, corresponding to the height of the beam at the midsection, is perturbed. The percent error is listed in Table 2, and a plot of the results is shown in Fig. 3.

In the preceding two cases, only one design variable is perturbed at a time. However, in optimization, simultaneous changes in more than one variable is common; hence, it is important to see how these various approximations handle the coupling in design variables.

Case 3

The design variables x_1 and x_2, corresponding to the height of the beam at the wall and midsection, are perturbed simultaneously. The percent error is listed in Table 3, and a plot of the results is shown in Fig. 4.

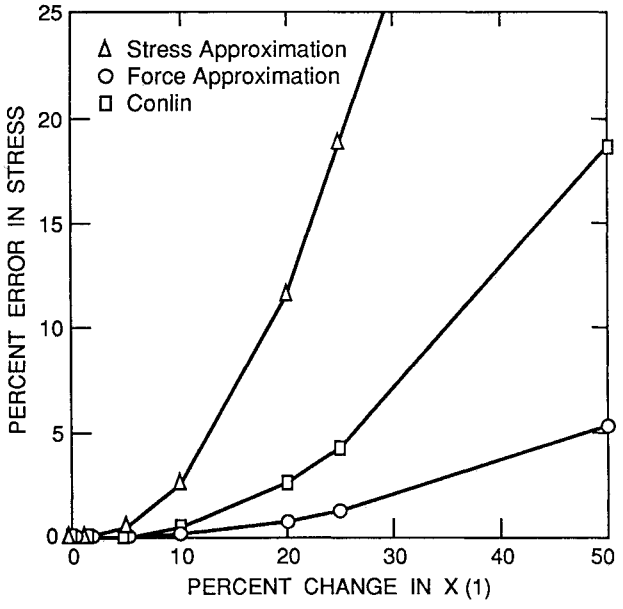

Fig. 2. Percent error in stress (x_1).

Table 1 % Error in stress, (design variable x_1)

Stress	$X_0 = \begin{Bmatrix} X_{01} \\ X_{02} \\ X_{03} \end{Bmatrix}$	$X_{01} +$ $0.01X_{01}$	$X_{01} +$ $0.05X_{01}$	$X_{01} +$ $0.10X_{01}$	$X_{01} +$ $0.20X_{01}$	$X_{01} +$ $0.25X_{01}$	$X_{01} +$ $0.50X_{01}$
σ_s	0.0	0.0	0.54	2.54	11.52	18.76	87.63
σ_e	0.0	0.0	0.048	0.48	2.58	4.24	18.65
σ_f	0.0	0.0	0.029	0.159	0.76	1.23	5.26

Table 2 % Error in stress, (design variable x_2)

Stress	$X_0 = \begin{Bmatrix} X_{01} \\ X_{02} \\ X_{03} \end{Bmatrix}$	$X_{02} +$ $0.01X_{02}$	$X_{02} +$ $0.05X_{02}$	$X_{02} +$ $0.10X_{02}$	$X_{02} +$ $0.20X_{02}$	$X_{02} +$ $0.25X_{02}$	$X_{02} +$ $0.50X_{02}$
σ_s	0.0	0.0	0.577	2.62	11.60	18.80	86.78
σ_c	0.0	0.0	0.08	0.57	2.74	4.43	18.91
σ_f	0.0	0.0	0.14	0.57	2.16	3.32	12.41

Table 3 % Error in stress, (design variables x_1 and x_2)

Stress	$X_0 = \begin{Bmatrix} X_{01} \\ X_{02} \\ X_{03} \end{Bmatrix}$	$X_{01} - 0.10X_{01}$ $X_{02} + 0.10X_{02}$	$X_{01} - 0.20X_{01}$ $X_{02} + 0.20X_{02}$	$X_{01} - 0.30X_{01}$ $X_{02} + 0.30X_{02}$	$X_{01} - 0.40X_{01}$ $X_{02} + 0.40X_{02}$	$X_{01} - 0.5X_{01}$ $X_{02} + 0.5X_{02}$
σ_s	0.0	2.57	8.98	18.38	29.94	42.93
σ_c	0.0	0.773	2.445	5.14	8.93	14.02
σ_f	0.0	0.163	0.44	0.79	1.15	1.51

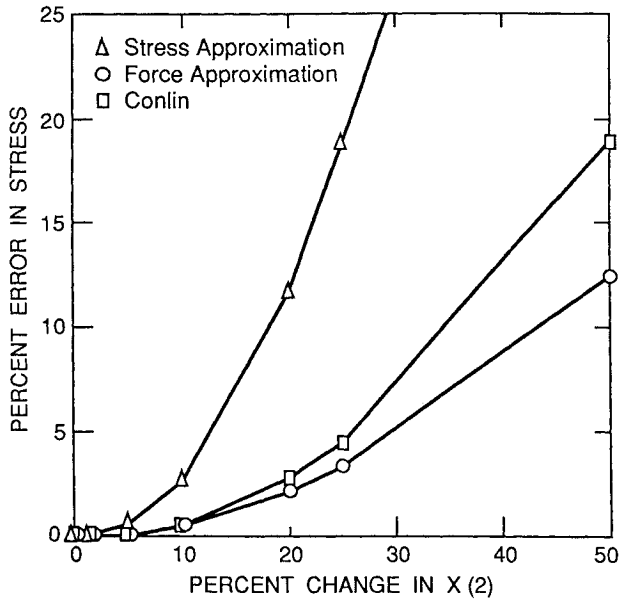

Fig. 3. Percent error in stress (x_2).

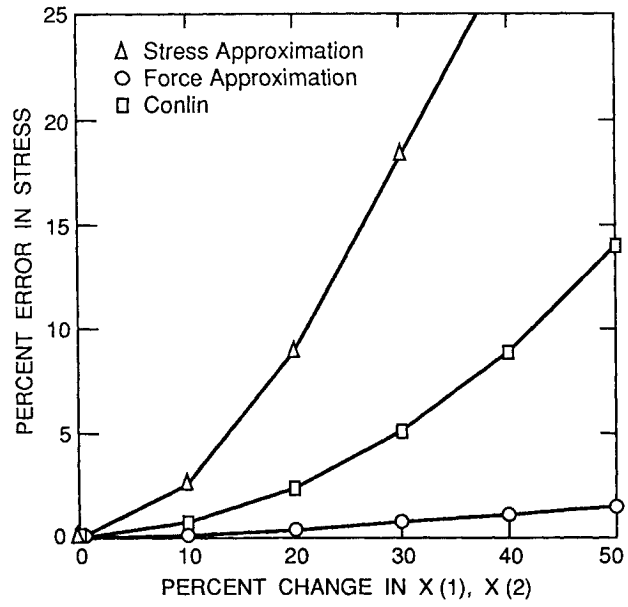

Fig. 4. Percent error in stress (x_1, x_2).

If x_1 is changed by $+50\%$ and x_2 by -50%, the errors are 77, 0.24, and 3.2% for $\{\sigma_s\}$, $\{\sigma_c\}$ and $\{\sigma_f\}$, respectively.

From these results, it is seen that, in general, the force approximation method is a significant improvement over previous methods. Although this simple example suggests that, when two variables are changed (Table 3), the force approximation is improved relative to a single variable, this is not considered to be a general conclusion. However, it is reasonable to conclude that the force approximation method deals well with the coupling that exists when more than one variable is changed.

Implementation

The approximation method outlined here is implemented on a Micro-VAX II computer as well as a Cray-XMP/48 using a modified version of the SAP IV program for finite-element analysis[9] and the ADS and DOT programs for design optimization.[10,11] The required gradients were calculated using a finite-difference routine.

The Method of Feasible Directions, programmed in ADS, is used in this study to solve the approximate problem.[12] The main advantage of this method is that it requires only the gradients of the active and the violated constraints during the optimization process. The newly developed DOT is also used to solve the engine-connecting rod example, and the results obtained are compared with those of ADS and Ref. 4.

The shape optimization program structure is shown in Fig. 5.

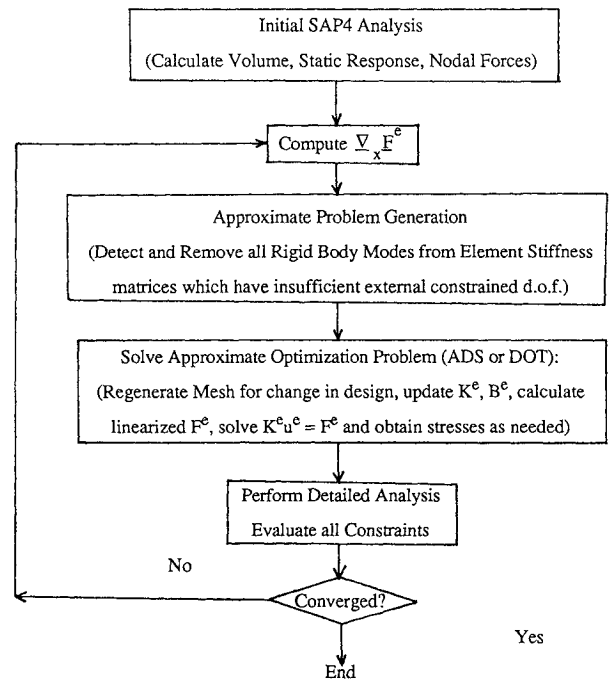

Fig. 5. Shape optimization program structure.

Table 4 Initial and final designs for cantilever beam

Design variable	Initial	Final			
		Case 1.1	Case 1.2	Case 1.3	Ref. 4
1	8.0	5.154	5.224	5.192	5.006
2	8.0	3.540	3.662	3.650	3.618
3	8.0	1.63	1.397	1.251	1.440
Volume, mm^3	8000.0	3487.85	3510.0	3496.11	3487.0
Iterations	—	5	4	6	10
Constraint violation, %		2.1	—	—	3.7

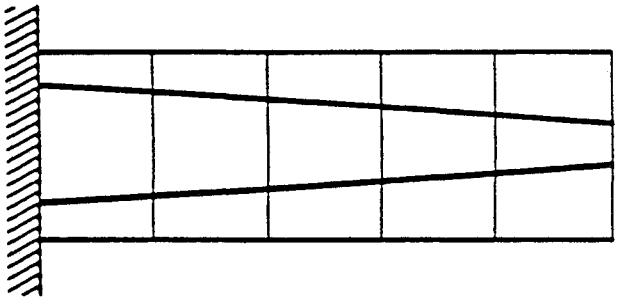

Fig. 6. Initial and final designs (three-dimensional beam).

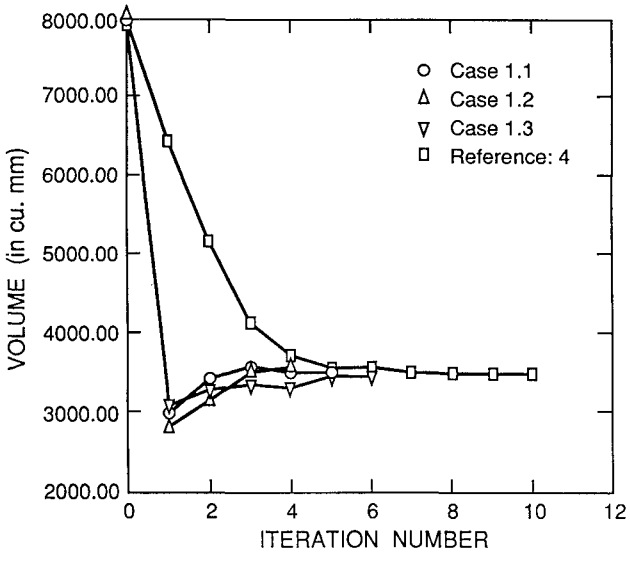

Fig. 7. Volume design history of three-dimensional cantilever beam.

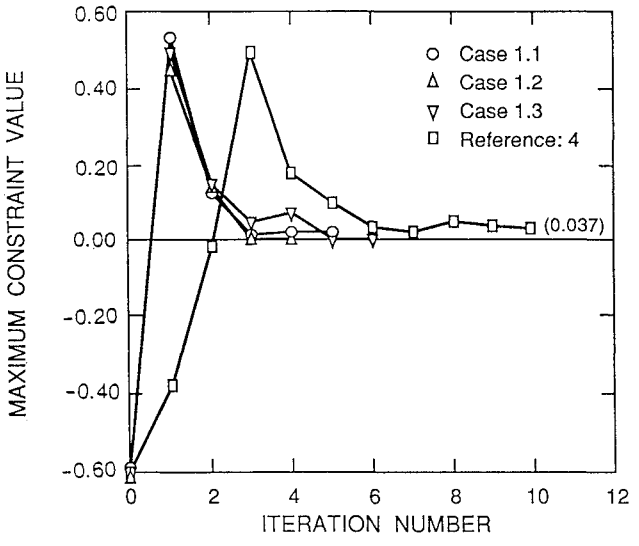

Fig. 8. Constraint design history of three-dimensional cantilever beam.

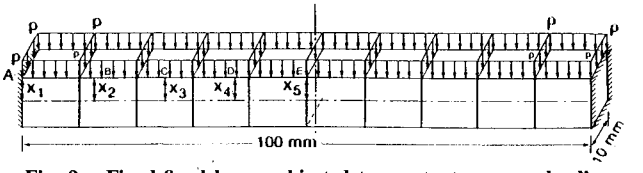

Fig. 9. Fixed-fixed beam subjected to constant pressure loading.

Numerical Examples

Several examples are offered here to demonstrate the proposed method. In each case, initial move limits of 80% were used at the beginning of the optimization process. These were reduced to 40% during the optimization. At the optimum, no move limits were active for any of the examples.

Case 1.1: Three-Dimensional Cantilever Beam

The classical example of a cantilever beam with a load at the free end is solved using this technique. The beam was modeled with five 20-node isoparametric hexahedron elements. A concentrated load of 10,000 N is applied at the free end. The dimensions of the model and the design variables are shown in Fig. 1. The material properties are as follows: Young's modulus = 10.0×10^6 MPa, Poisson's ratio = 0.3, and allowable normal stress = 3000 MPa. The height of the upper surface of the beam from the midplane is varied to find the optimum shape. The width of the beam is constant. Since there is symmetry about the xz plane, the shape of the lower surface is symmetric with the upper one. The shape of the upper surface was determined using a quadratic fit through the three key locations of the form

$$y = a_0 + a_1 x + a_2 x^2$$

where a_0, a_1 and a_2 are determined from the x and y locations of points A, B, and C. The optimization results are given in Table 4, where one iteration corresponds to a complete cycle through the program. Case 1.1 is solved on a Micro-VAX II computer using the ADS optimization program. The final shape, iteration history, and the bending stress constraint violations are shown in Figs. 6, 7, and 8, respectively.

Case 1.2

On a Cray-XMP/48, this problem is solved using 4 iterations with an optimum objective function of 3510.0 mm^3 and no violation of the stress constraints.

Case 1.3

The preceding results were obtained using a Jacobi technique to detect the rigid-body modes in the element stiffness matrices. The same problem was also repeated by arresting a set of 6 degrees of freedom (since there are 6 rigid-body modes in space). The problem converged in 6 iterations with an optimum volume of 3496.11 mm^3.

Case 2: Fixed-Fixed Beam

The fixed-fixed beam structure shown in Fig. 9 is modeled with 10 20-node isoparametric hexahedron elements and is subjected to a constant pressure, prescribed directly by means of pressure intensities at the face corner nodes. This example demonstrates the application of this method to a statically indeterminate structure, and a higher-order polynomial is also used to determine the shape of the surface. The dimensions of the structure and the design variables are shown in Fig. 9. The material properties are as follows: Young's modulus = 10.0×10^6 MPa, Poisson's ratio = 0.3, and allowable normal stress = 3000 MPa. The upper and lower surfaces of the beam are varied to obtain the optimum shape, and the width of the beam is constant. Considering symmetry about the xz plane, the shape of the top surface determines the shape of the whole structure. An interpolating polynomial by the Lagrangian method is fit through the five key locations shown in Fig. 9.

A brief outline of the Lagrangian method follows, where the approximating polynomial is

$$p(x) = \sum_{k=0}^{n} L_k(x) f_k$$

where

$$L_k(x) = \sum_{\substack{j=0 \\ j \neq k}}^{n} (X - X_j) \Big/ \prod_{\substack{j=0 \\ j \neq k}}^{n} (X_k - X_j)$$

and f_k is the function values of n given points.

The initial and final design variables are shown in Table 5, and Figs. 10, 11, and 12 show the final design, volume-iteration curve, and stress constraint violations, respectively. This problem is solved using the ADS program on a Micro-Vax II computer.

Case 3.1: Engine-Connecting Rod

The engine-connecting rod is a critical automobile part, which connects the reciprocating piston to the rotating crankshaft. The shape optimal design of this part was solved earlier by Yoo et al.[13] using a two-dimensional plane stress finite-element model and by Yang and Botkin,[4] who used a

Table 5 Initial and final designs for fixed-fixed beam

Design variable	Initial	Final
1	8.0	5.204
2	8.0	3.4093
3	8.0	1.7918
4	8.0	2.0933
5	8.0	2.6778
Volume, mm^3	16,000.0	5615.816
Iterations	—	6
Violation, %	—	—

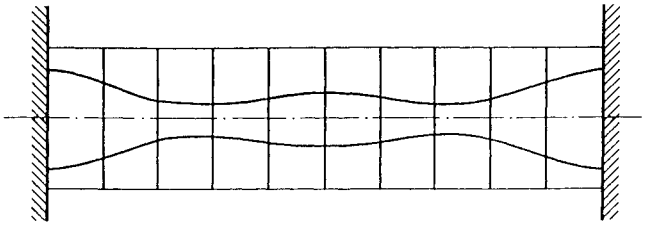

Fig. 10. Initial and final design of fixed-fixed beam.

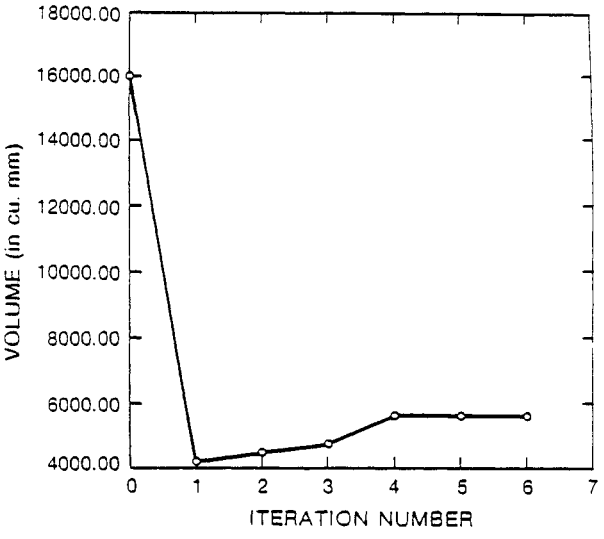

Fig. 11. Volume design history of fixed-fixed beam.

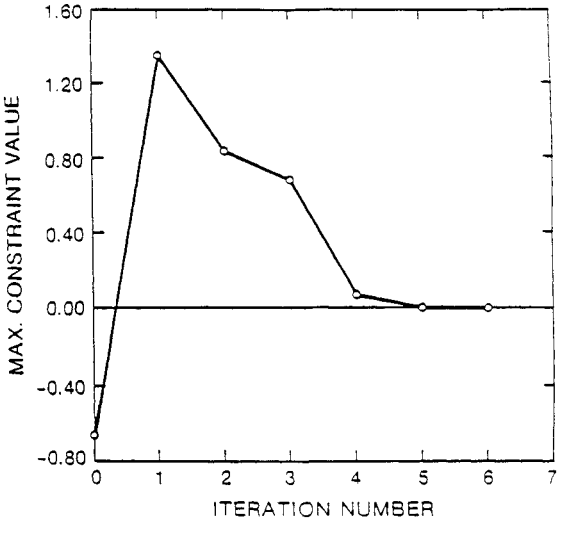

Fig. 12. Constraint design history of fixed-fixed beam.

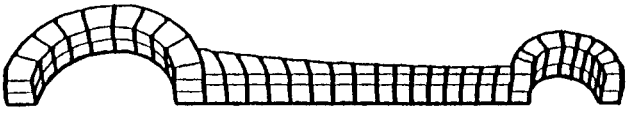

Fig. 13. Finite-element model of engine-connecting rod.

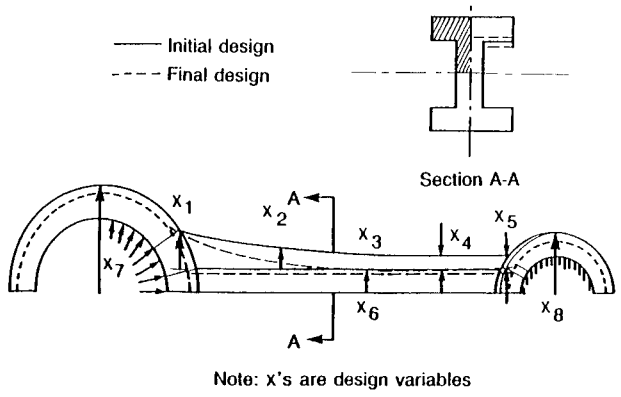

Fig. 14. Design model of engine-connecting rod.

three-dimensional solid model. In this study, the authors use the same finite-element mesh, materials, loads, and design model used in Ref. 4. The only exception is that a slightly different mesh-generation scheme was used to relate the design model to the analysis model.

The connecting rod, shown in Fig. 13, is modeled with 105 solid, 20-node isoparametric elements and has a total of 2126 degrees of freedom. Considering symmetry, only one-fourth of the connecting rod needs to be modeled. The right hole (piston side), which connects to the piston, is fixed to eliminate rigid-body motion. The material properties are as follows: Young's modulus = 10.0×10^6 MPa, Poisson's ratio = 0.3, and yield stress limit (octahedral shear stress) = 3000 MPa. The rod is subjected to high cyclic loads varying from high compressive loads due to combustion to high tensile loads due to inertia. Here, an arbitrarily selected pressure of 3000 MPa is applied, varying from 0 to 90 deg at the left hole.

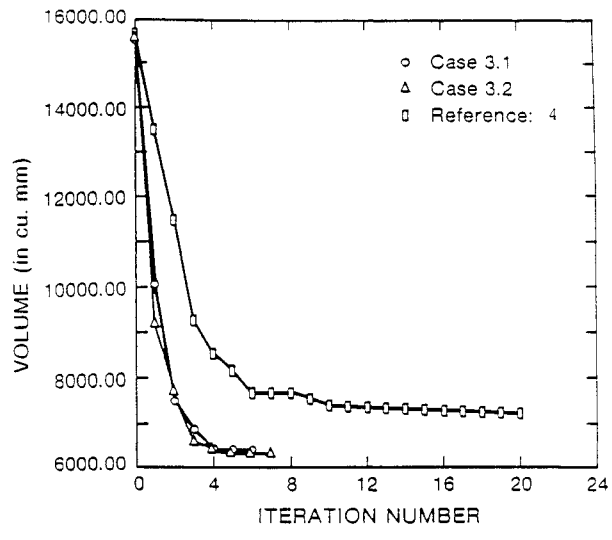

Fig. 15. Volume design history of connecting rod.

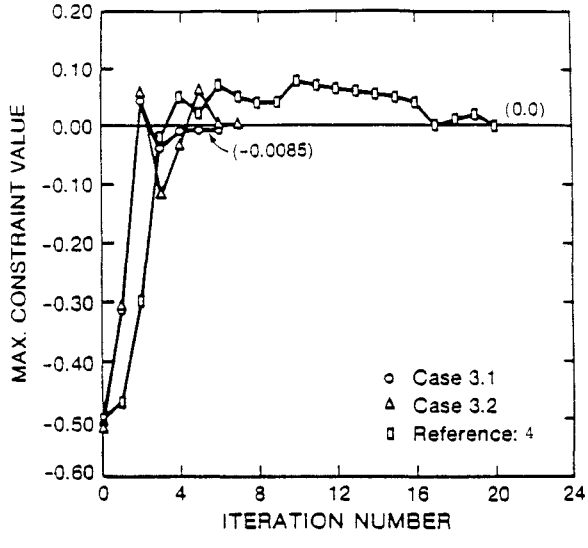

Fig. 16. Constraint design history of connecting rod.

Table 6 Initial and final designs for engine-connecting rod

Design variable	Initial	Final		
		Case 3.1	Case 3.2	Ref. 4
1	10.956	12.284	12.360	12.512
2	6.3700	2.2239	2.2370	2.8478
3	3.9667	1.6115	1.2015	1.4220
4	3.0024	0.8772	0.6811	1.0964
5	3.2711	1.4418	1.1631	1.2733
6	6.8156	5.4265	5.5374	7.2219
7	31.271	26.044	25.995	26.461
8	17.553	13.300	13.300	13.300
Volume, mm^3	15531.0[a]	6410.6	6296.3	7217.8
Iterations		6	7	20
Violation, %		—	—	—

[a]The initial volume in Ref. 4 is 15,686.7 mm^3. This slight difference is due to different mesh-generation schemes used by the two studies.

Eight design variables are used to find the optimum shape—one each for the outer radii of the right and left holes, one for the height of the web, and the remaining five to design the shape of the shank and neck regions (Fig. 14). Octahedral shear-stress constraints are imposed at various locations of each element consistent with Ref. 4.

Case 3.1 is solved on a Cray-XMP/48 using the ADS program.

Case 3.2

Here, DOT is used to solve the same problem on a Cray-XMP/48. A total of seven approximate iterations are required to converge to an optimum volume of 6296.15 mm^3.

The initial and final designs are shown in Table 6, and Figs. 15 and 16 show the iteration history and stress constraint violations.

Conclusions

The concept of using force approximations at the element joints is shown to improve the efficiency of the shape optimization problem. From the constraint history plots, it is evident that this approximation method is of higher quality than other existing methods for stress constraints. Since this approximation has a wide applicable range in the design variable space, the use of large move limits is possible and this accelerates the convergence to the optimum. Also, even with the large move limits used here, the stress approximations were sufficiently accurate to overcome constraint violations quickly. The approximate problem is relatively expensive since it requires repeated element-level stress recovery calculations. Research is continuing to reduce the cost of the approximate problem through further nested approximations.

By taking advantage of this high-quality approximation, the total number of iterations required for structural shape optimization can be reduced by a factor of 3 or more, resulting in the same level of efficiency achieved previously in sizing problems.

Acknowledgments

This research was supported by NASA Grant NAG 1567, CRAY Research, Inc., Minnesota, and the MacNeal-Schwendler Corporation, California.

References

[1]Lust, R. V. and Schmit, L. A., "Alternative Approximation Concepts for Space Frame Synthesis," NASA CR 172526, March 1985.

[2]Vanderplaats, G. N. and Salajegheh, E., "A New Approximation Method for Stress Constraints in Structural Synthesis," *Proceedings of the AIAA/ASME/ASCE/AHS 28th Structures, Structural Dynamics and Materials Conference*, AIAA, Washington, DC, 1987, pp. 314–321.

[3]Kodiyalam, S., "Shape Optimization of Three-Dimensional Continuum Structures Using Efficient Approximation Methods," Ph.D. Dissertation, Univ. of California, Santa Barbara, CA, June 1988.

[4]Yang, R. J. and Botkin, M. E., "A Modular Approach for Three-Dimensional Shape Optimization of Structures," *AIAA Journal*, Vol. 25, March 1987, pp. 492–497.

[5]Gallagher, R. H., *Finite Element Analysis Fundamentals*, Prentice-Hall, Englewood Cliffs, NJ, 1975.

[6]Carnaghan, B., Luther, H. A., and Wilkes, J. O. *Applied Numerical Methods*, Wiley, New York, 1969.

[7]Przemieniecki, J. S., *Theory of Matrix Structural Analysis*, McGraw-Hill, New York, 1968.

[8]Fleury, C. and Braibant, V., "Structural Optimization: A New Dual Method Using Mixed Variables," *International Journal for Numerical Methods in Engineering*, Vol. 23, No. 3, 1986, pp. 409–429.

[9]"SAP-IV—A Structural Analysis Program," Univ. of California, Berkeley, CA., Rept. EERC 73–11, June 1973.

[10]Vanderplaats, G. N. and Sugimoto, H., "A General Purpose Optimization Program for Engineering Design," *International Journal of Computers and Structures*, Vol. 24, No. 1, 1986, pp. 13–21.

[11]Hansen, S. R., Vanderplaats, G. N., and Miura, H., "MICRO-DOT—Users Manual," Engineering Design Optimization, Inc., Santa Barbara, CA, 1986.

[12]Vanderplaats, G. N., *Numerical Optimization Techniques for Engineering Design: with Applications*, McGraw-Hill, New York, 1984.

[13]Yoo, Y. M., Haug, E. J., and Choi, K. K., "Shape Optimal Design of an Engine Connecting Rod," *Journal of Mechanisms, Transmissions, and Automation in Design*, Vol. 106/415, Sept. 1984, pp. 415–419.